Iodinated X-ray contrast agents: Photoinduced transformation and monitoring in surface water

Iodinated X-ray contrast agents: photoinduced transformation and monitoring in surface water

D. Fabbri[1], P. Calza[1], D. Dalmasso[1,2], P. Chiarelli[2], V. Santoro[3], C. Medana[3]

(1) Department of Chemistry, University of Torino, via P. Giuria 5, 10125 Torino, Italy

(2) Department of Chemistry, Loyola University, Chicago, IL, 60660

(3) Department of Molecular Biotechnology and Health Sciences, University of Torino, via P. Giuria 5, 10125 Torino, Italy

Abstract

Conventional wastewater treatment methods have shown to be unsuitable for a complete elimination of iodinated X-ray contrast agents (ICMs), which have thus been found in wastewater treatment plant (WWTP) effluent and in surface water. Once in the surface water, they could be transformed through different processes and form several transformation products that may need to be monitored as well. To this end, we studied the abatement and transformation of ICMs by combining laboratory experiments with in field analyses. We irradiated different aqueous solutions of the selected pollutants in the presence of TiO_2 as photocatalyst, aimed to promote ICMs degradation and to generate photoinduced transformation products (TPs) similar to those occurring in the environment and effluent wastewater. This experimental strategy has been applied to the study of three ICMs, namely iopromide, iopamidol and diatrizoate. A total of twenty-four, ten, and ten TPs were detected from iopamidol, diatrizoate and iopromide, respectively. The analyses were performed using a liquid chromatography-LTQ-FT-Orbitrap mass spectrometer. The mineralization process and acute toxicity evolution were assessed as well over time and revealed a lack of mineralization for all ICMs and the formation of harmful byproducts.

After characterizing these transformation products, WWTP effluent and surface water taken from several branches of the Chicago River were analyzed for ICMs and their TPs. HRMS with MS/MS fragmentation was used as a confirmatory step for proper identification of compounds in water and wastewater samples. All three of ICM were detected in the effluent and surface water samples, while no significant amount of TPs were detected.

Keywords: X-ray contrast agents, transformation products, wastewater, TiO_2, HRMS

1. Introduction

Every year between 40 and 80 million doses of iodinated X-ray contrast agents (ICMs) are used for diagnostic purposes, the estimated annual production is more than 5000 tons (Wendel et al 2014, Gharekhanloo and Torabian 2012). ICMs are excreted mainly un-metabolized (>90%) (Wendel et al 2014), so most of the drug dose enters urban wastewater after urinary elimination. Their abatement is partly achieved in secondary anoxic or anaerobic treatment, while only a small percentage is removed under aerobic conditions (Busetti, et al. 2008). The yields of removal for nonionic contrast agents *via* ozonation in water treatment plants are 35-55% and even less than 20% for ionic ones (Seitz et al 2008; Putschew et al 2007). Reverse osmosis systems are used to remove absorbable organic halide (Drewes et al, 2001). Iopamidol and diatrizoate are stable with respect to chlorination, while iopamidol is not. (Wendel et al 2014). Filtration-based treatments, biotransformation (Kormos, et al 2010) or direct photolysis (Doll and Frimmel 2003, Sichel et al 2011) have been proposed as well; however, these methods require long treatment times and exhibit low efficiency.

Due to their wide use, high biochemical stability, and low yields of abatement in treatment plants, elevated concentrations of ICMs have been detected in hospital and domestic wastewater, treated wastewater effluent (Redeker et al 2014), surface water, groundwater and drinking water (Węgrzyn and Żabczyński, 2014; Ternes and Hirsch, 2000; Stuart et al 2012, Kase et al 2011, Watanabe et al. 2016).

In the present study, we focus on the photocatalyzed transformation of three ICMs: iopamidol, iopromide and diatrizoate. Iopamidol (IO) is one of the most popular and widely used non-ionic ICMs worldwide. This molecule has a good solubility in water, with a partition coefficient ($LogP_{OW}$) of -2.09 and a distribution coefficient ($logD_{OW}$, pH 7.4) of -2.31 (Pitrè and Felder 1980). Standard activated sludge treatment may remove up to 35% of IO (Ternes and Hirsch, 2000, Ternes et al., 2007, Kormos et al., 2011). The concentration of IO in effluent from hospitals and municipal WWTPs are high and ranged from 0.2 to 16 µg/L (Ternes et al., 2003, Busetti et al., 2010, Kormos et al., 2011). As a result the concentration of IO in river water that is fed with this effluent may be as high as 0.386 µg/L (Bruchet et al., 2005) and >0.5 µg/L (Seitz et al., 2006). Actually, iopamidol has also been frequently detected at high concentrations (2.7-3.3µg/L) in the source water processed into drinking water (Duirk et al., 2011, Simazaki et al., 2015). Iopamidol is also thought to be the major precursor of iodinated disinfection byproducts (Duirk et al, 2011).

Iopromide (IP) is a low osmolality, non-ionic contrast agent and one of the most common molecules used in diagnostic radiology; the production of iopromide alone is about 130 tons per year (Ning et al 2008). The $LogP_{OW}$ value for iopromide is -2.95, while the $logD_{OW}$ (pH 7.4) is equal to -2.12 (Pitrè and Felder 1980). It is refractory to common wastewater treatment (Kalsch et al 1999) and is frequently detected in surface water, groundwater and soils (Schulz et al 2008, Perez et al 2006), as well as in effluent from urban areas near hospital complex in concentrations from ng/L to µg/L (Pitrè and Felder 1980, Santos et al 2013).

Diatrizoate (DTZ), a ionic ICM, has a $LogP_{OW}$, 1.53 and $logD_{OW}$ (pH 7.4) equal to -2.53, indicating a high solubility in water (Pitrè and Felder 1980). It is essentially non-biodegradable (Seitz et al 2008) and was detected in surface water and groundwater at concentrations up to 1 µg/L (Howard and Muir 2011). Coated biofilm reactors (Hapeshi et al 2013) and advanced oxidation processes (AOP, Polo et al, 2016) have been tested for treatment of wastewater containing DTZ as well.

To date, only a few studies of ICM transformation products have been carried out. Eleven TPs were prioritized and their structures elucidated by HRMS and NMR, using a screening approach not dependent upon the availability of standards (Zonja et al 2015). LC-QTOF-MS (Singh et al. 2015) coupled with the statistical tools was used to identify TPs at environmentally relevant conditions. In this approach, unspiked wastewater samples were collected and analyzed for the presence of iopromide and its putative TPs.

Photocatalytic treatment processes using titanium dioxide (TiO_2) hold promise for treating contaminated water with highly recalcitrant organic contaminants. Ionic ICMs like diatrizoate that had shown to be remarkably resistant to biotransformation (Kalsch et al 1999, Haiss and Kümmerer 2006) but may be degraded by photocatalytic treatment. At present, only a few studies concerning the photocatalytic treatment of ICM have been undertaken. Doll and Frimmel (2004 and 2005) studied the photocatalytic degradation of nonionic ICM (iomeprol and iopromide), suggesting significant ICM degradation and release of iodine substituents from the central ring structure, but with only a limited mineralization of organic carbon. Some transformation products of iopromide have been generated by UV/H_2O_2 (Singh et al. 2015).

Heterogeneous photocatalysis is widely used not only to achieve the decontamination of aquatic systems, but also to simulate the abiotic transformation of pollutants occurring in the euphotic zone leading to potentially harmful transformation products. In the present study, we aim to investigate the whole ICM degradation process by studying the transformation products, the mineralization process and the toxicity of the system. Initially, laboratory experiments were performed to artificially produce transformation compounds similar to those formed in oxido/reductive pathways by adopting a photocatalytic process as a model system. This approach was previously successfully used and permitted to identify several TPs, alongside the parent compounds, in water samples (Calza et al 2010, 2011, and 2013).

In a second phase, we analyze WWTP effluent and searched for all ICMs and their transformation products.

2. Experimental section

2.1. Materials and Reagents

N,N'-Bis(1,3-dihydroxy-2-propanyl)-2,4,6-triiodo-5-(lactoylamino)isophthalamide (Iopamidol, IO), 3,5-bis(acetylamino)-2,4,6-triiodobenzoic acid (Diatrizoate, DTZ, ≥ 98.0%), 1-*N*,3-*N*-*bis*(2,3-dihydroxypropyl)-2,4,6-triiodo-5-(2-methoxyacetamido)-1-*N*-methylbenzene-1,3-dicarboxamide (Iopromide, IP, ≥ 98.0 %),

acetonitrile (≥99.9%), acetonitrile (≥99.9%), formic acid (99%) and phosphoric acid were purchased from Sigma Aldrich, Italy. All aqueous solutions were prepared with ultrapure water Millipore Milli-Q™.

TiO_2 P25 (Evonik Industries, Italy) was used as photocatalyst, after being subjected to irradiation and washings with ultrapure water in order to eliminate the potential interference caused by adsorbed ions such as chloride, sulfate and sodium. In all photocatalytic experiments, TiO_2 was used at a loading of 200 mg L^{-1}.

2.2. Irradiation procedures

Irradiation experiments were performed in stirred cylindrical closed cells (40 mm i.d. x 25 mm, made of Pyrex glass) on 5 ml of aqueous dispersions containing 20 mgL^{-1} of each analyte and 1000 mg L^{-1} of TiO_2. A Blacklight Philips TLK 05 (40W) lamp source with emission maximum at 360 nm was employed for irradiation.

The dispersions were collected from the cells at the end of the programmed irradiation period and then were filtered through 0.45 µM Millex LCR hydrophilic PTFE membranes (Millipore) before the analysis.

2.3. Analytical procedures

2.3.1. Liquid Chromatography-MS

All samples were analyzed by HPLC/HRMS. The chromatographic separations, monitored using an MS analyzer, were carried out with a Phenomenex Luna C18 (2) 150 × 2.1 mm × 3 µm particle size (Phenomenex, Bologna, Italy), using an Ultimate 3000 HPLC instrument (Dionex, Thermo Scientific, Milan, Italy). The Injection volume was 20 µL and the flow rate 200 µL/min. The following gradient mobile phase composition was adopted: 5/95 to 100/0 in 40 min acetonitrile/formic acid 0.05 % v/v in water when run on ESI positive mode or acetonitrile/ammonium acetate /0.1 mM in the negative ion mode.

A LTQ Orbitrap mass spectrometer (Thermo Scientific, Milan, Italy) equipped with an atmospheric pressure interface and an ESI ion source was used. The LC column effluent was delivered into the ion source using nitrogen as both sheath and auxiliary gas. The capillary voltage and tube lens voltage in the ESI source were maintained at 37.00 V and 65 V, respectively. The source voltage was set to 3.5 kV (in both positive and negative ion mode). The capillary temperature was maintained at 275°C. The acquisition method used was optimized beforehand in the tuning sections for the parent compound (capillary, magnetic lenses and collimating octapole voltages) to achieve maximum sensitivity. Mass accuracy of recorded ions (vs calculated) was ± 20 millimass units (mmu, without internal calibration). APCI conditions were as follows: capillary temperature 250°C; APCI vaporizer temperature 450°C; source voltage 6.00 V; source current 5.00 uA; capillary voltage 2.00 V (-10.00 V negative ions); tube lens 80.00 V (-118.00 V negative ions).

Analyses were run using full scan MS (50-1000 *m/z* range), MS^2 acquisition in the positive ion mode, with a resolution of 30000 (500 *m/*z FWHM) in FTMS (full transmission) mode. Product ion studies were carried

out in positive ion mode rather than negative because a wider distribution of structure-specific fragment ions were observed. The ions submitted to MS^2 acquisition were chosen on the base of full MS spectra abundance without using automatic dependendent scan. Collision energy was set to 30 % for all of the MS^2 acquisition methods. MS^2 acquisition range was between the values of ion trap cut-off and *m/z* of the $(M+H)^+$ ion. Xcalibur (Thermo Scientific, Milan, Italy) software was used both for acquisition and data analysis. For each ICM, we have built a calibration curve over 5 points ranging from 10 to 5000 µg/L in ultrapure MilliQ water, river water and real wastewater. Linearity and selectivity were verified. No significant matrix effect was observed neither at lower nor at higher concentration level. We selected an instrumental LLOQ value of 10 µg/L for each ICM after checking that the signal/noise ratio was > 10 (see Table S1).

2.3.2. Ion chromatography

Ammonium ions formed during the mineralization process were analysed with a Dionex instrument equipped with a conductometer detector and a CS12A column. Methanesulphonic acid (25 mM) was used as the eluent at a flow rate of 1 mL min^{-1}. In such conditions, the retention time of the ammonium ion was 4.7 min. Anions (iodide, nitrate and nitrite) were analysed with an AS9HC anionic column and a mobile phase composed of $NaHCO_3$ (12 mM) and K_2CO_3 (5mM) at a flow rate of 1 mL min^{-1}. Under these experimental conditions, the retention times of nitrite, nitrate and iodide were 7.35, 10.92 and 24.52 min, respectively.

2.3.3. Total organic carbon analyzer

Total organic carbon (TOC) was measured in filtered suspensions using a Shimadzu TOC-5000 analyzer (catalytic oxidation on Pt at 680°C). The calibration was performed using potassium phthalate standards.

2.3.4. Toxicity Measurements

The toxicity of reaction mixtures collected at different irradiation times was evaluated with a Microtox Model 500 Toxicity Analyzer (Milan, Italy). Acute toxicity was evaluated with a bioluminescence inhibition assay using the marine bacterium *Vibrio fischeri* by monitoring changes in the natural emission of the luminescent bacteria when challenged with toxic compounds. Freeze-dried bacteria, reconstitution solution, diluent (2% NaCl) and an adjustment solution (non-toxic 22% sodium chloride) were obtained from Azur (Milan, Italy). Samples were tested in a medium containing 2% sodium chloride, in five dilutions, and luminescence was recorded after 5, 15, and 30 min of incubation at 15°C. Since no substantial change in luminescence was observed between 5 and 30 minutes, only the percent toxicity recorded at 15 minutes will be discussed. Inhibition of luminescence, compared with a toxic-free control to give the percentage inhibition, was calculated following the established protocol using the Microtox calculation program.

170

171 **2.4. Sample preparation**

172 Real water samples (river water and wastewater) were collected at two sites close to the city center of
173 Chicago (Illinois, U.S.A), in a sampling campaign performed from March to May 2015.

174 The locations and dates of sampling are summarized in Table 1. Sampling sites other than water treatment
175 plants (Bertau and Weed Street) were selected due to their proximity to hospitals and ease of access to the
176 shoreline of the river. The site called Weed Street is downstream from a cluster of hospitals that include
177 Memorial Hospital, Northwestern Memorial Hospital, Olson Hospital, the Rehabilitation Institute of
178 Chicago, and Veterans Lakeside Medical Center. The site called Berteau (Intersection of Berteau Ave. and
179 Montrose Ave.) is near Kindred and Forkosh Hospitals adjacent to Lincoln West Medical Center. The
180 Chicago River flows from Lake Michigan inland. The direction of the Chicago River was reversed in the early
181 part of the 20th century to prevent pollution in the river from contaminating the drinking water intake
182 portals in Lake Michigan. Effluent water samples were acquired from the Stickney Wastewater Treatment
183 Plant (WWTP) and the Kirie WWTP in the Chicago metropolitan area to determine if Iodine contrast media
184 compounds or their transformation products were entering the Chicago River from the WWTPs. Maps of
185 these sites are shown in Figure S1. The first is the Chicago's newest facility, is fully automated and serves a
186 predominantly residential area, with a capacity of 272 million liters of wastewater per day. The Stickney
187 Water Reclamation Plant is the largest wastewater treatment facility in the world. The Plant serves 2.38
188 million people in a ca. 670 square kilometers area including the central part of Chicago and 43 suburban
189 communities. In these facilities, wastewater undergoes a number of physical and chemical cleaning
190 processes that include sedimentation, coagulation, and sand filtration. In the Kirie Water Reclamation Plant
191 disinfection with sodium hypochlorite is carried out from 30 April to 30 October when outdoor water
192 recreation activities occur. For this reasons the first sample (called Kirie Before) was collected in April
193 without having undergone chlorination and a second sample (called Kirie After) after chlorination.

194 The pH of the wastewater samples were 7.3 (Kirie Before), 6.9 (Kirie After), and 7.1 (Stickney). The pH
195 value of the Chicago River water samples collected at the four sites below ranged from 6.1 to 6.5.

196 The samples were filtered using 8 µm Whatman Glass microfiber filters, Grade GF and formic acid added in
197 order to reach pH=2.

198 All samples were concentrated by solid-phase extraction (SPE) using Oasis HLB 5cc Glass Vac Cartridge (200
199 mg sorbent, 60 mm particle side, Waters Corp, Milford, MA, USA). They were conditioned with 6 ml CH_3OH
200 added with 0.25% (v/v) of formic acid followed by 5 mL of ultrapure water.

201 Water samples (500 mL), spiked with 500 µL isoxsuprine (1 mg/L) used as recovery standard (Ohmori et al.
202 2008), were percolated through the cartridge at a flow rate 10 mL/min. Elution was performed with 6 mL
203 of 0.25 % (v/v, w/w) formic acid in CH_3OH. Eluates were concentrated to 100 µL under nitrogen flux and
204 reconstituted with 200 µL of 20 % CH_3OH (v/v) in water, then directly analyzed by HPLC-MS.

Quantitative data were obtained with an external calibration after normalization on isoxsuprine signal. We routinely use isoxsuprine as internal standard aimed to evaluate the instrumental response fluctuations. Limit of detection after concentration on SPE cartridges were 0.5, 0.7 and 1 ng/L for IP, IO and DTZ, respectively. The same extraction procedure was applied to a standard mixture analysis of an ultrapure water and real waste water sample spiked with target molecules. The same procedure was applied to each ICM subjected to illumination in ultrapure water and wastewater, aimed to establish the recovery of ICMs and their photogenerated TPs following SPE; the analysis of photo-degradation mixture was performed before and after SPE. The extraction recovery was >90 % percentage for all of the parent molecules studied. Considering TPs, for IO and IP recovery ranges from 60 to 85% for most of TPs, with the exception of TP involving the ring closure, for which recovery was 5-10%. For DTZ, recovery of TPs still holding the carboxylic group and with several hydroxyl groups were 30-70%, while TPs involving ring closure was 5-20%.

3. Results and discussion

3.1. ICMs degradation and toxicity assessment

ICMs were irradiated under UV-A light in the presence of TiO_2 P25 and analyses were run in the ESI positive ion mode, suitable both for the parent compounds and for most of the photogenerated products. The degradation curves for ICM compounds are plotted in Figure 1 and show that several hours of irradiation are required for their complete degradation. Iopromide degrades the fastest ($t_{1/2}$ 30 min), while diatrizoate is the most refractory ($t_{1/2}$ 2h). Complete degradation was achieved after 8, 16 and 24 h for IP, IO and DTZ, respectively.

The TOC profiles suggested an initial fast degradation followed by a slower TOC decrease as irradiation times increased; in all cases, the complete mineralization was not achieved even after 48 h of irradiation (Fig. 1). The mineralization of Iopamidol proceeded quickly; during the first two hours of irradiation almost 55% of the initial TOC was abated. Afterwards, the mineralization slowed down and 10% of TOC persisted at the end of the 48 h period. A similar TOC trend was also observed for iopromide, where almost 50% is degraded within 2h, then TOC slowly decreases until only 15% persisted. Diatrizoate is the ICM with lowest extent of mineralization (40% remains after 48 h) and showed the slowest degradation rate as well.

Most of the Iodine atoms were recovered as iodide ions (around 75%), while the fate of nitrogen was more complex, slow, and similar for all ICMs. The release of nitrogen is initially very fast and within a few hours almost 50-60% of the stoichiometric amount is mineralized, as expected mainly as ammonium ions (Calza et al, 2005). At longer irradiation times the recovery slightly increased but for all ICMs complete nitrogen mineralization was not achieved; a residual of almost 30-40% still remains bound to organic carbon.

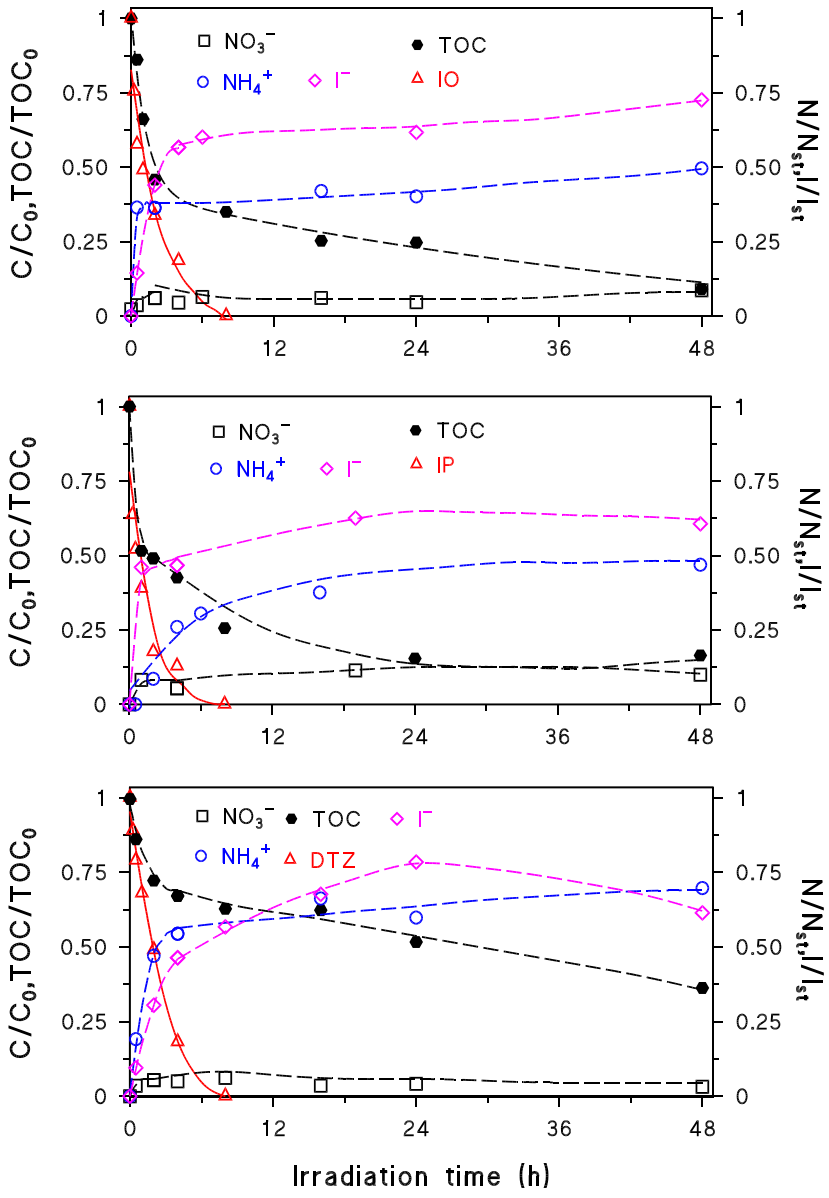

Figure 1. TOC profile and iodine and nitrogen release over time: (top) iopamidol, (middle) iopromide and (bottom) diatrizoate.

Acute toxicity was evaluated as well by monitoring changes in the natural emission of the luminescent bacteria *Vibrio fischeri* when exposed to potentially toxic compounds. Out of the various available bioassays, this test is sensitive, rapid, cost effective, reproducible and it can be used for almost all kind of toxic compounds (Parvez et al, 2006, Matsushita et al, 2015). The toxicity was expressed as percentage of inhibition of the bacteria luminescence. Results obtained on samples subjected to different irradiation times are plotted in Figure 2. A clear correlation exists for all ICMS between their degradation and the progressive increase in the toxicity. Acute toxicity increased from 0 min onward, so assessing that while ICMs are not toxic, their transformation proceeded through the formation of toxic compounds. This shape suggested the formation of harmful compounds during the different stages of ICMs transformation but, in

particular, the species formed in the last stages of degradation seemed to be more toxic ones. The study of DTZ degradation by solar radiation in the presence of H_2O_2 conducted by Polo et al (2016) reported a relationship between increased percentage DTZ abatement and a greater inhibition luminescence of *Vibrio fischeri*.

Wendel et al (2016) has demonstrated that the chlorination of iopamidol produces low molecular weight transformation products that account for the majority of the observed toxicity. Furthermore, we checked the toxicity of all inorganic ions possibly formed, namely cyanate, nitrate, nitrite, ammonium, iodate, iodide, and all exhibit no effect. Therefore, the measured toxicity cannot be ascribed to the released inorganic ions.

The test with *Vibrio fischeri* performed on standard solutions of the released inorganic anions allow us to exclude their contribution to the observed increased toxicity. Duirk et al 2011 observed a similar toxicity increase when using cells as organism and they attribute it to the formation of iodo-halomethanes and iodo-acetic acids. Although the bioluminescence inhibition test is different from cytotoxicity assay used by Duirk et al 2011, it cannot excluded that part of this observed toxicity could be attributed to the formation of iodo-acetic acids.

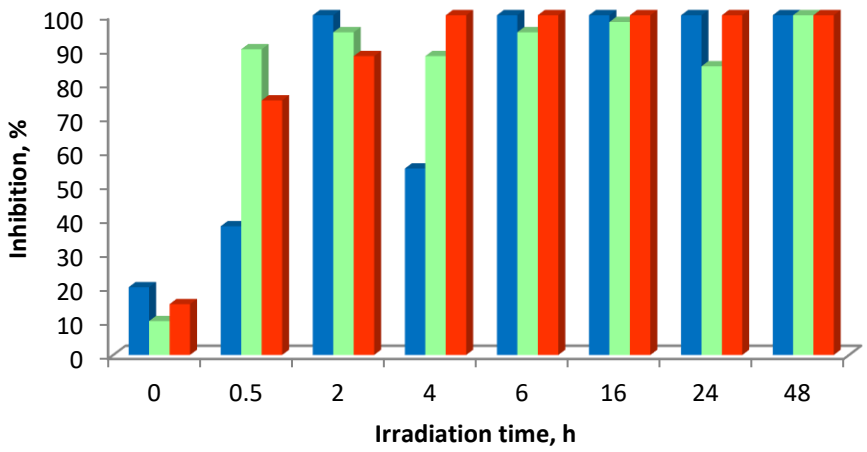

Figure 2. Inhibition percentage over time: ■ Iopamidol, ■ Iopromide and ■ Diatrizoate.

3.2. *ICMs transformation pathways*

3.2.1. Iopamidol

The photocatalytic degradation of IO yields twenty-four transformation products presented below. Table 2 summarizes the measured masses and most probable empirical formulas of all TPs, while their evolution profiles are provided in Figure 3 (main TPs) and Figure S2 (secondary TPs).

Thirteen of the degradation products were identified in the present study for the first time and their empirical formulas were assigned by HRMS analysis. Structural features of the transformation products were investigated by MS^2 studies, presented in Tables S2-S6 and in Spectra S1-S13.

The most common ion formation processes involve losses of iodine atoms, HI, NH_3, H_2O, CO, HCO, and H_2CO that do not provide a great deal of structural information and thus permit to recognize TPs only at level 3 (Schymanski et al. 2014). This occurs for TPs **IO-505**, **IO-487, IO-332**, **IO-331**, **IO-636**, **IO-577**, **IO-454**, **IO-794** and **IO-541**, whose MS^2 spectra and structural features are reported in SI (see spectra S5-S13).

Conversely, TPs **IO-385**, **IO-367**, **IO-580** and **IO-615** yield product ion spectra that demonstrate side-chain specific fragmentation and permitted to attribute a structure with an higher confident level; for these, the structural-diagnostic ions are presented and discussed below. **IO-385** and **IO-367** are suggested to be formed by cyclization involving the loss of HI part of the A-side chain in iopamidol. The product ion spectrum of **IO-385** demonstrates fragmentation that is specific for the cyclized ring containing an oxygen atom (see spectra S1). The fragment ion at 313.9 *m/z* was formed by the cleavage of the bond between an aromatic carbon and oxygen and the amide bond in the fused ring followed by the transfer of hydrogen from the ion to the $C_3H_4O_2$ neutral formed. The TP **IO-367** has a structure that is similar to that of **IO-385** except the oxygen atom in the ether ring that is replaced by a pi-bonding carbon atom. It does not exhibit the fragmentation pathway that produces a $C_3H_4O_2$ neutral; this observation supports the proposed structure of **IO-367**.

The species 579.9407 *m/z* (**IO-580**) is indicated by accurate mass analysis to have the empirical formula $C_{14}H_{20}O_6N_3I_2$. This ion undergoes a side chain specific cleavage of a nitrogen –carbon bond to lose $C_3H_6O_2$ (1-propene-1,3-diol), from either the A or A' side chain after the transfer of a hydrogen atom to the charge-baring fragment. Product ions formed by the losses of smaller molecules (NH_3 and CH_3OH) are observed as well (spectrum S3), so assessing the presence of a primary amine and a primary alcohol.

The species 614.7746 m/z (**IO-615**) with empirical formula $C_{11}H_{10}O_4N_2I_3$ is generated by the loss of the side chain B and by the loss of one of the side chains A/A during photocatalytic transformation. The side chain A/A' is observed to undergo a loss of $C_3H_5O_2$ by cleavage of the carbon nitrogen bond in this side chain to form an ion at product ion 541.7227 *m/z*. This side chain has a terminal aldehyde and alcohol, instead of two hydroxyl groups as the fragmentation of **IO-580**, so the neutral fragment lost has less hydrogen. These evidenced allowed to recognize this structure at level 2 (Schymanski et al. 2014). An ion at 486.8626 *m/z*, resulting from the loss of HI is observed as well (spectrum S4).

Schemes 1-2 show the proposed structures for all identified TPs. Transformation products appear to be formed by different pathways, described by one or more reactions characterizing the path itself, and their formation involved:

- Deiodination and oxidation: **IO-652**, **IO-650**, **IO-636**, **IO-580**, **IO-577**, **IO-545**, **IO-505**, **IO-487**, **IO-385**, **IO-367**, **IO-332** and **IO-331**;

- Detachment of the amidic chain: **IO-736**, **IO-706**, **IO-662** and **IO-632**;
- Reversal of the amidic chain: **IO-779**, **IO-778** and **IO-705**;
- Detachment of the side chains: **IO-615** and **IO-541**;
- Oxidation: **IO-794** and **IO-776**;
- Dimerization: **IO-1407**.

The initial pathways are mainly oxidative, involving the attachment of hydroxy groups to alkyl side chains, the conversion of alcohols to carbonyl and carboxylic acid groups, and the replacement of iodine with H/OH groups.

Twelve transformation products underwent a de-iodination reaction, a process known to easily occur both in AOPs and chlorination treatments (Singh et al 2015, Zhao et al. 2014, Tian et al 2014) and are presented in Scheme 1. The deiodination process could involve attack at one of the iodine sites with: (1) dissociative electron attachment, as seen with iomeprol (Jeong et al. 2010); (2) concomitant attachment on the side chain with ring closure. Two of them, namely **IO-650** and **IO-652,** are known to be formed *via* direct photolysis (Tian et al 2014), and **IO-652** also under UV-Fe(III) (Zhao et al. 2014), while the others were identified for the first time in this study. Four mono-iodinated compounds, namely **IO-385**, **IO-331**, **IO-332** and **IO-367** are detected and their formation could involve iopamidol cyclization on the side chains. A tentative structure is proposed in Scheme 1.

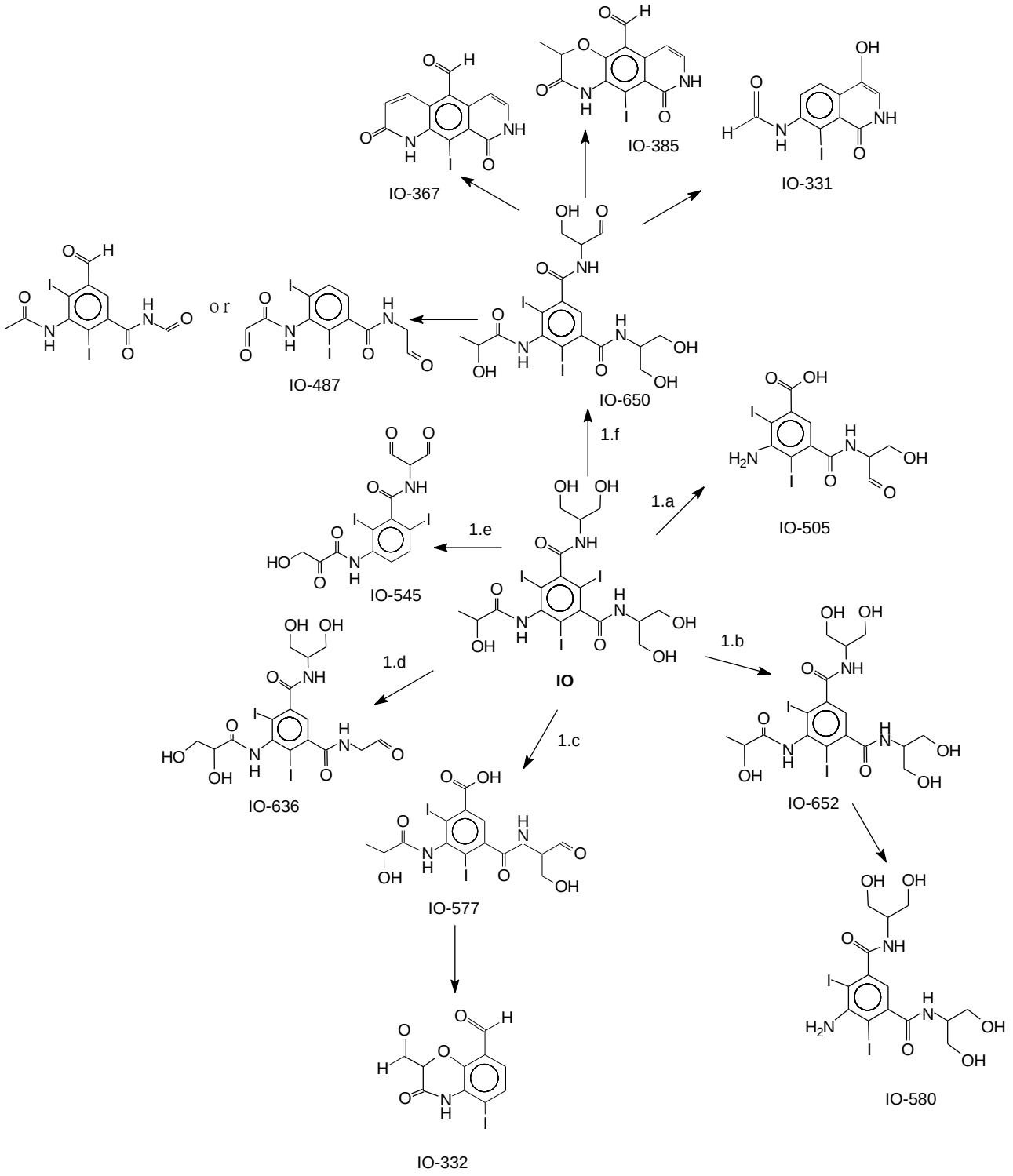

Scheme 1. Transformation pathways of iopamidol in the presence of TiO_2 P25 - part I -due to de-iodination and oxidation processes.

Transformation pathways not involving deiodination were observed as well in this study. Most of these pathways were recognized during chlorination treatment as well (Wendel et al 2014; Singh et al 2015) and are reported in Scheme 2. Two products formed by the oxidation of the molecule without deiodination were detected. While **IO-776** formation is known to occur during H_2O_2/UV treatment (Singh et al 2015), **IO-**

794 is identified for the first time in this study (path 2.e). The formation of a dimeric product occurred, named **IO-1407** in path 2.d and is known to also occur during the chlorination process (Wendel et al 2014). Four products, referred to as **IO-706**, **IO-736**, **IO-662** and **IO-632** in path 2.c and 2.f, are derived from the detachment of the amidic side chain. Two derivatives (**IO-736**, **IO-662**) were detected as well and could match with nitro derivatives (Wendel et al. 2014); a further detachment of the amino group leads to the TP **IO-615**.

Three species resulting from the inversion of amide side chain B were identified in path 2.b (**IO-779**, **IO-778** and **IO-705**), all known to be formed from oxidative chlorination treatment (Singh et al 2015). We observed that the primary amine groups formed as a result of side chain reversal were rapidly converted to carboxylic acids (Wendel et al. 2014).

The TP formation profiles suggest some preferential degradation pathways. The products **IO-650** (*m/z* 649.9467) and **IO-331** (*m/z* 330.9549), path 1.f, **IO-794** (*m/z* 793.8632) path 2.e and **IO-541** (*m/z* 540.7379) path 2.b. are among the most abundant products and are plotted in Figure 3 (top). **IO-331** and **IO-541** appear to be the most abundant and persistent TPs; the maximum yields of **IO-541** and **IO-331** were reached between one and two hours of irradiation, decreasing only after 4 hours of degradation. The formation of **IO-650** product appears particularly fast, formed through the loss of HI and the oxidation of the substrate to give the **IO-794** product, whose maximum concentration was reached after 30 min. The product **IO-545** reaches the maximum concentration after an hour of irradiation. Some smaller TPs were also formed, in most cases were found to be quite resistant to photocatalytic treatment, as they persisted for several hours (see **IO-331** and **IO-541** products for example).

The TPs recognized were degraded within 6h, while a certain percentage of nitrogen and organic carbon remained. These results mirror the TOC curve shown in Figure 1, where a sharp decrease occurred within 4 h, when the transformation products with known empirical formulas completely disappeared. No TPs were observed in samples analyzed after longer irradiation times. These analyses were performed by HPLC-MS analysis in both APCI and ESI, positive and negative mode, but no TPs were detected. Therefore, the high toxicity registered at long irradiation time cannot be ascribed to any of these TPs, but to some smaller organic nitrogen-containing TPs.

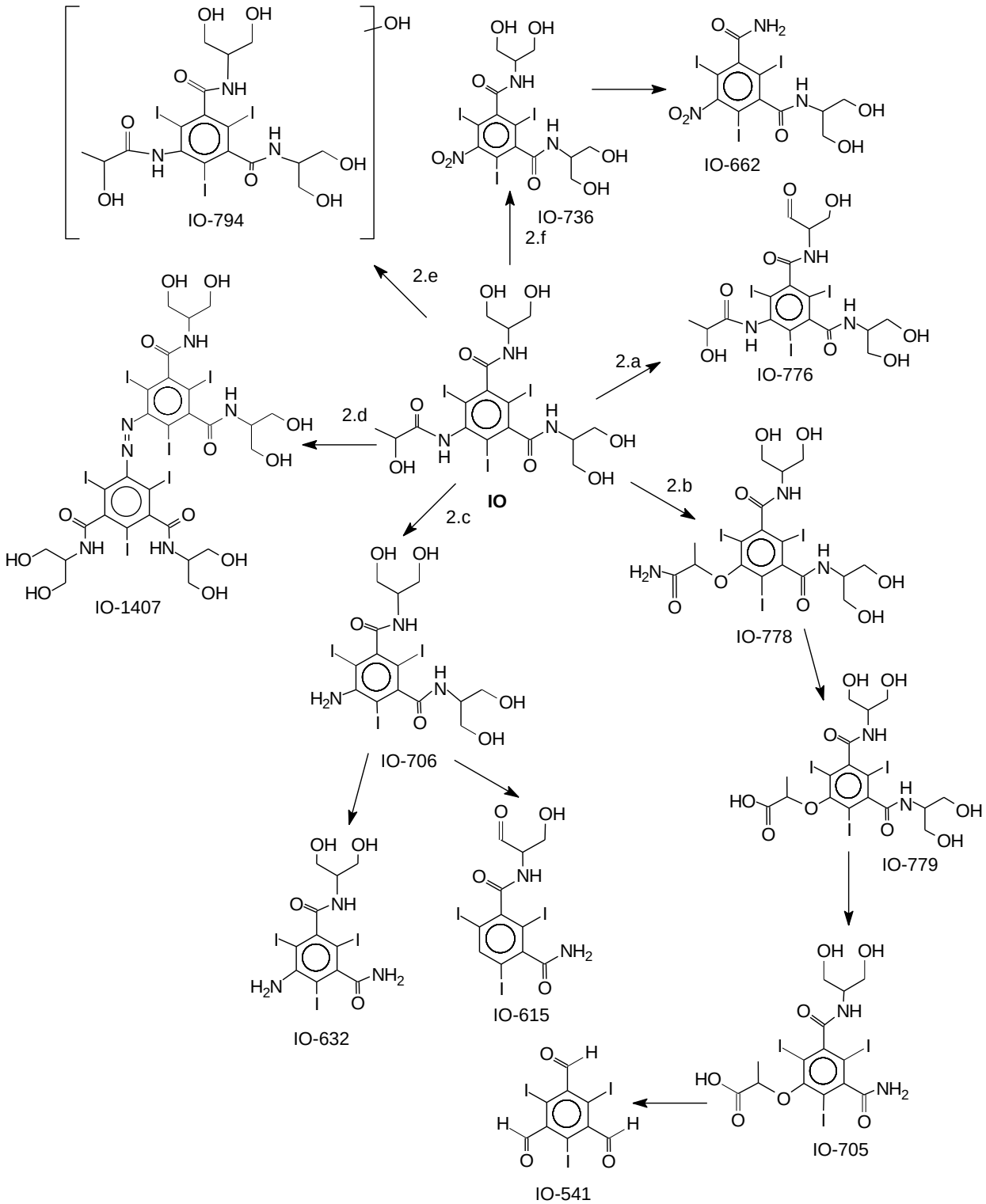

361

362 **Scheme 2**. Transformation pathways of iopamidol in the presence of TiO_2 P25- part II.

363

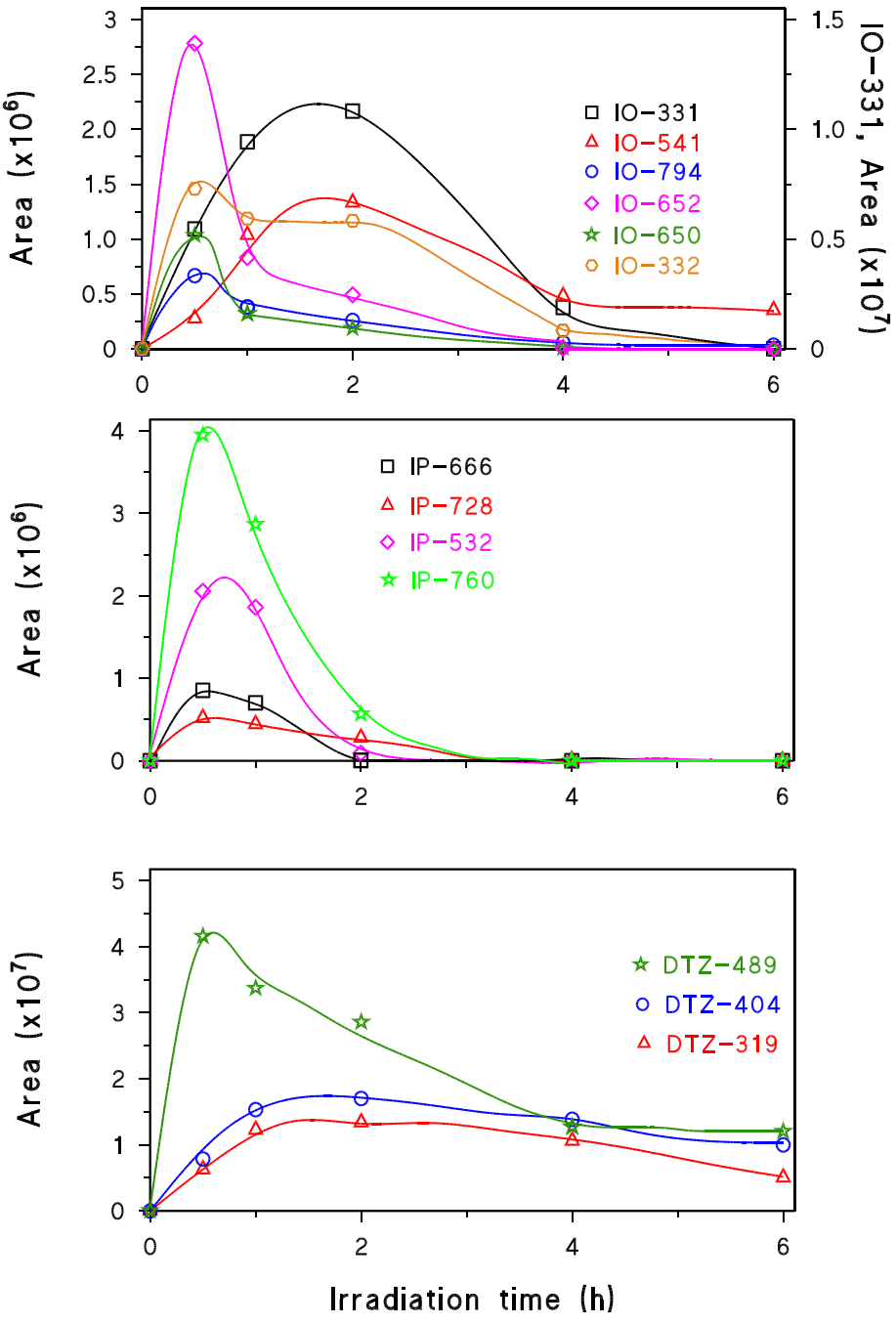

364

365

366

367 **Figure 3**. Main time-dependent transformation profiles for IO (top), IP (middle) and DTZ (bottom).

368

369 *3.2.2. Iopromide*

370 Ten TPs were detected during iopromide degradation; seven of these TPs are known to be formed during
371 solar light irradiation (Pérez et al 2009, Zonia et al 2015), while the other three are recognized here for the
372 first time. All TPs are presented in Table 3, while MS^2 product ions are reported in Tables S7-S9; MS^2 spectra
373 for newly detected compounds are shown in supporting information as Spectra S14-S16.

The TP **IP-760** formed by degradation of Iopromide gives a protonated ion at 759.8520 *m/z* with the empirical formula $C_{17}H_{21}O_7N_3I_3$. This precursor ion undergoes a side chain specific cleavages to form product ions at 686.7899 formed by the cleavage of the nitrogen-carbonyl carbon bond in the A side chain (see spectrum S14). The ion 572.8942 *m/z* is formed by the loss of HI which may include a hydrogen atom from one the hydroxy groups on the B side chain causing the B chain to cyclize and eliminate C_2H_5ON from the cyclic structure by cleavage of nitrogen-carbonyl carbon bonds and the carbon-carbon bond [HOH_2C – COC(aromatic)]. The TP **IP-728** (empirical formula $C_{16}H_{17}O_6N_3I_3$) fragments to lose C_2H_5ON by cleaving the nitrogen-carbonyl carbon bond in the B side chain to form a product ion at 668.7861 (see spectrum S15). The product ion at 654.7702 m/z is formed by the cleavage of the same bond in the A chain (loss C_3H_7ON). These MS^2 evidences allowed to attribute to **IP-760** and **IP-728** a structure at level 2 (Schymanski et al. 2014). The TP **IP-532** does not present in MS^2 spectrum structural diagnostic product ions (spectrum S16) and it can be only attributed at level 4 (Schymanski et al. 2014).

The comprehensive mechanism of transformation is inclusive of all pathways and is presented in Scheme 3. It comprises:

- Triiodinated compounds, namely **IP-760** and **IP-728**;
- Diiodinated compounds, **IP-682**, **IP-666**, **IP-652** and **IP-532**;
- Monoiodinated and de-iodinated compounds **IP-554**, **IP-526**, **IP-466** and **IP-452**.

Eight de-iodinated compounds were identified and formed through two concomitant initial pathways. Four TPs involved mono-deiodination; three of them are known from the literature (**IP-682**, **IP-666** and **IP-652**) (Pérez et al 2009, Zonia et al 2015), while one product has been identified for the first time in the present study (**IP-532**).

Pathway 1 begins with the de-iodination of the molecule, followed by side chain oxidation. Subsequently, the structure loses part of the chain. This is followed by demethylation of amidic nitrogen on the side chain and this is observed together with de-iodination and loss of part of the side-chain. Four mono-iodinated or de-iodinated species were detected, all known to be formed *via* exposure to simulated solar radiation (Pérez et al 2009, Zonja et al 2015); they are **IP-554**, **IP-526**, **IP-466** and **IP-452**. Pathway 2 shows oxidative de-iodination leading to the formation of **IP-682**. Pathway 3 does not involve de-iodination but provides for the gradual shortening of the side chains.

The temporal profiles for main TPs are presented in Figure 3 (middle), while the temporal profiles associated with the other TPs are shown in Figure S3. The evolution profiles of de-iodinated compounds show their maximum concentration at times ranging from 30 min to 1 h, in agreement with the release of iodine plotted in Figure 1: the species **IP-760** is the main TP. Two TPs, namely **IP-760** and **IP-728** are formed through these routes and are identified for the first time in this study. They reach the maximum yield after 1 hour and decrease over the next 2-3 hours, in agreement with the temporal decrease in TOC. The toxicity profile maximized after 48 h, time at which all recognized TPs are degraded but a TOC residue is registered.

At that irradiation time, we performed HPLC-MS analysis in APCI and ESI, positive and negative mode, but no TPs were detected. Again, the contribution to toxicity has to be ascribed to small molecules, not detected in the present study.

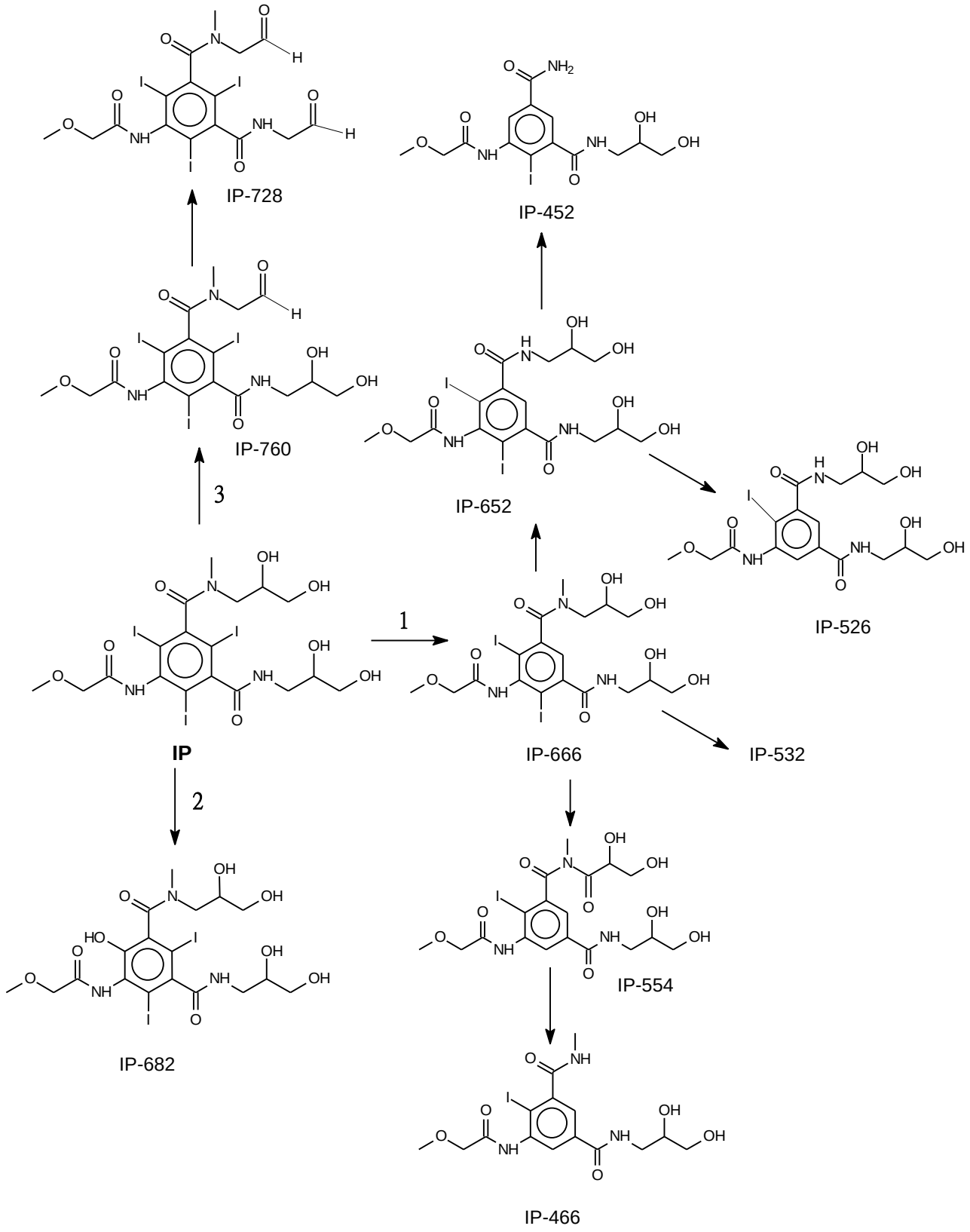

Scheme 3. Transformation pathways of iopromide in the presence of TiO_2 P25.

3.2.3. Diatrizoate

The photocatalytic degradation of diatrizoate produced ten transformation products, five of which are recognized for the first time in this study. The masses and empirical formulas of all DTZ TPs are presented in Table 4, while Tables S10-S12 summarize their MS^2 fragmentation; their MS^2 spectra are reported as well in SI (spectra S17-S19). Two of them, namely **DTZ-404** and **DTZ-631**, gave no MS^2 signals and their characterization is then limited to level 4. Three of them show some peculiar MS^2 losses (**DTZ-471**, **DTZ-333** and **DTZ-319**) and are discussed on SI. However, MS^2 evidences are not enough to attribute a structure at level 2 and, we can characterize them at level 3 (Schymanski et al. 2014).

All transformation products already known from literature are formed through a photoinduced degradation. TPs marked as **DTZ-574** and **DTZ-489** match with the TPs products formed under UV irradiation (Rastogi et al 2014), while species **DTZ-587**, **DTZ-487** and **DTZ-574** were previously identified in the presence of TiO_2 (Sugihara et al 2013). Scheme 4 shows the overall degradation routes and the transformations involve:

- Path 1, hydroxylation/decarboxylation: **DTZ-587** and **DTZ-404**;
- Path 2, deiodination: **DTZ-489**, **DTZ-319** and **DTZ-363**;
- Path 3, deiodination and cyclization: **DTZ-487**, **DTZ-471**, and **DTZ-333**;
- Path 4, hydroxylation/chain cleavage: **DTZ-631**, and **DTZ-574**

The observed degradation paths are mostly oxidative, with the exception of deiodination products, whose formation involved a reductive pathway. Methyl groups and aromatic ring in the ICM are hydroxylated (**DTZ-631**, **DTZ-587** and **DTZ-404**). In some cases, the cyclization involving one of the side chains can occur, resulting in the loss of HI from DTZ, to form **DTZ-487** from which either **DTZ-333** or **DTZ-471** may be formed. Other mono- or diiodinated TPs were detected as well, that may undergo more degradation pathways (**DTZ-319**). Decarboxylation of the acid substituent occurred in **DTZ-587**, **DTZ-404** and **DTZ-333**.

Four transformation products are formed by oxidation, more or less extended, and deiodination and all of them were detected for the first time in the present study (namely **DTZ-471**, **DTZ-404**, **DTZ-333** and **DTZ-319**).

Three transformation products involved deiodination (**DTZ-489**, **DTZ-487** and **DTZ-363**), all already known from the literature (Rastogi et al 2014, Sugihara et al 2013). Path 4 leads to **DTZ-487**, which can then lose iodine or a water molecule; it finally eliminates HI cyclizing on the aromatic ring and producing the species

DTZ-471. Path 2 involves di-deiodination and a partial loss of the side chains, whereas path 1 proceeds via decarboxylation, subsequently deiodination and detachment of the side chains.

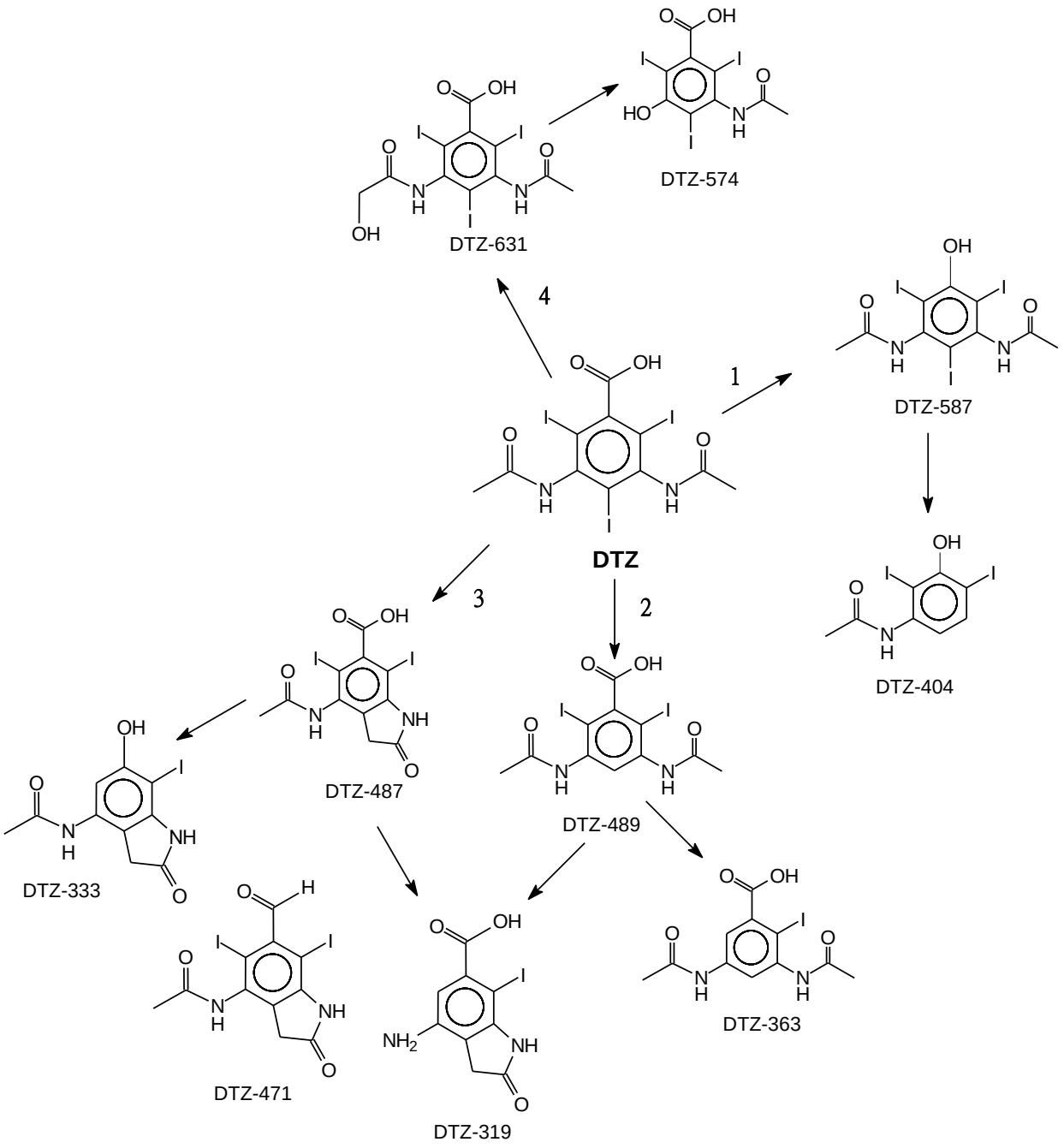

Scheme 4. Transformation pathways of diatrizoate in the presence of TiO_2 P25.

Figure 3 (bottom) and Figure S4 depict the time evolution profiles of TPs. The main TPS are **DTZ-489** and **DTZ-319**, formed through path 2 and **DTZ-404**, involving pathway 1. **DTZ-489** is easily formed and achieved the maximum amount after 30 min of irradiation, **DTZ-404** and **319** showed a maximum at 2 hours of irradiation. Most of other TPs are formed within 1 h or 2 h, but then are slowly degraded. As an example, the concentration of the **DTZ-471** increases up to 8 hours of degradation. The slow degradation of TPs is in agreement with the TOC curve shown in Figure 1, where the mineralization process results very slow and

455 limited. Toxicity is not directly linked with the detected TPs and, similar to the other ICMs, could be
456 attributed to the formation of some small molecule.

457 **3.3. ICMs research in wastewater and river water**

458 Treatment plant effluent and river water acquired in the Chicago metropolitan area sampled in the Spring
459 and Summer of 2015 were analyzed for ICM and their TPs. Table 5 shows the concentrations found for the
460 three ICMs substrates in the different wastewater and river water samples analyzed. The most abundant
461 compound detected was iopamidol confirming the widespread use of this X-contrast agent in North
462 America. None of the transformation products generated by photolysis in the presence of TiO_2 were
463 detected in any river water or wastewater sample that was analyzed.
464 ICM released from local hospitals into a local sewer may enter natural water sources without passing
465 through a treatment plant. Most local sewers in the Chicago area (and in older cities around the world)
466 were built over a century ago before wastewater treatment was carried out. Sewer systems such as these
467 were originally designed to direct a limited amount of storm water and sewage into different waterways or
468 Lake Michigan directly (www.vah.com, 2016). These local sewers are now connected to the Chicago area
469 Metropolitan Water Reclamation District (MWRD) intercepting sewers (built after the local sewer system)
470 that direct the flow from the local sewers to the treatment plants. These local sewers are required to
471 transport more water today than when they were first built, and when they exceed their flow capacity
472 sewage will empty into natural waterways. Wastewater from homes and businesses (including hospitals
473 and medical centers) that enter local sewers may spill into natural waterways when the sewer is at high
474 capacity. This is most probable means of ICM entering the Chicago River and its tributaries. This would
475 explain why significant concentrations of Iopromide and Diatrizoate are observed in the water sample
476 taken at the Bertau site. Sewer overflows following rainstorms have been known to close Lake Michigan
477 Beaches in Chicago for brief periods of time due to bacterial contamination. Therefore it is conceivable that
478 ICM and other potential pollutants may enter natural water sources in the same way.
479 The concentrations of all three ICM, iopromide, Iopamidol, and Diatrizoate are much lower in the
480 chlorinated Kirie effluent sample relative to the unchlorinated Kirie effluent sample. The effluent water
481 sample taken from the Stickney WWTP was observed to have a large concentration of iopamidol relative to
482 the Kirie chlorinated sample and the Weed Street water sample, suggesting that iopamidol may pass
483 through conventional treatment processes. The concentrations of the ICM detected in the wastewater
484 effluent samples suggest that chlorination may be an effective means of breaking down ICM in wastewater
485 treatment. At the very least, the effluent water analyses suggest that analyzing chlorinated and
486 unchlorinated effluent for the reaction products of NaOCl with ICM may yield positive results after the
487 structures of these products are generated and determined in a laboratory.
488
489

3.4. Conclusions

Irradiation of three iodine contrast reagents (iopamidol, iopromide, and diatrizoic acid, collectively referred to as ICM) in the presence of TiO_2 produced forty-four transformation products (TPs), twenty-one of which had not been detected in any previous study. Toxicity assessments were carried out by exposing irradiated mixtures of TPs to bioluminescent bacteria, *Vibrio fischeri*. Some of the TPs formed were indicated to be toxic in this assay and, in particular, bioluminescence was strongly reduced when *Vibrio fischeri* bacteria was exposed to reaction mixtures irradiated for much longer periods of time (to the point of near mineralization), containing no detectable intermediate transformation products and only much smaller molecules. All three of iodine contrast reagents (ICM) were detected in wastewater effluent and natural water taken from different branches of the Chicago while no significant amounts of TPs formed by photo catalysis were detected. The analysis of wastewater effluent sampled at different times suggests that ICMs may be degraded during chlorination.

Acknowledgements

We acknowledge support from a Marie Curie International Research Staff Exchange Scheme Fellowship (PHOTOMAT, proposal no. 318899) within the 7th European Community Framework Programme and the project funded by MIUR, in the frame of the collaborative international consortium WATERJPI2013-MOTREM of the Water Challenges for a Changing World Joint Programming Initiative (WaterJPI) Pilot Call.

References

Bruchet A., Hochereau C., Picard C., Decottignies V., Rodrigues J.M., Janex-Habibi M.L. (2005) Analysis of drugs and personal care products in French source and drinking waters: the analytical challenge and examples of application. Water Sci. Technol. 52:53-61

Busetti F., Linge K. L., Blythe J. W., Heitz, A. (2008) Rapid analysis of iodinated X-ray contrast media in secondary and tertiary treated wastewater by direct injection liquid chromatography-tandem mass spectrometry; J. Chromatogr. A, 1213: 200–208

Busetti F., Linge K. L., Rodroguez C., Heitz, A. (2010) Occurrence of iodinated X-ray contrast media in indirect potable reuse systems. J. Enviro. Sci. Health, Part A, 45: 542–548

Calza P., Pelizzetti E., Minero C. (2005) The fate of organic nitrogen in photocatalysis: an overview J. Appl. Electrochem, 35:665–673

Calza P. , Marchisio S., Medana C., Baiocchi C. (2010) Fate of the Antibacterial Spiramycin in River Waters, Anal. Bioanal. Chem. 396: 1539–1550

523 Calza P., Medana C., Raso E., Giancotti V., Minero C. (2011) N,N-diethyl-m-toluamide transformations in
524 river water: Sci. Tot. Environ**.,** 409: 3894-3901
525 Calza P., Medana C., Padovano E., Giancotti V., Minero C. (2013) Fate of selected pharmaceuticals in River
526 waters, Environ. Sci. Pollut. Res, 20(4): 2262-227
527 Doll T.E., Frimmel F.H. (2003) Fate of pharmaceuticals - photodegradation by simulated solar UV-light.
528 Chemosphere 52: 1757-1769
529 Doll T.E., Frimmel F.H. (2004) Kinetic study of photocatalytic degradation of carbamazepine, clofibric acid,
530 iomeprol and iopromide assisted by different TiO_2 materials-determination of intermediates and reaction
531 pathways**.** Water Research 38: 955–964.
532 Doll T.E., Frimmel F.H. (2005) Removal of Selected Persistent Organic Pollutants by Heterogeneous
533 Photocatalysis Catalysis Today 101: 195–202.
534 Drewes J. E., Fox P., Jekel M. (2001) Occurrence of iodinated X-ray contrast media in domestic effluents and
535 their fate during indirect potable reuse Environ. Sci. Health Part A: Toxic/Hazard Subst. Environ. Eng. 36:
536 1633-1645
537 Duirk S. E., Lindell C., Cornelison C. C., Kormos J., Ternes T. A., Attene-Ramos M., Osiol J., Wagner E. D.,
538 Plewa M. J., Richardson S. D. (2011) Formation of Toxic Iodinated Disinfection By-Products from
539 Compounds Used in Medical Imaging, Environ Sci Technol. 15;45(16):6845-54
540 Gharekhanloo F., Torabian S. (2012) Comparison of Allergic Adverse Effects and Contrast Enhancement
541 Between Iodixanol and Iopromide; Iran. J. Radiol. 9 (2): 73-76
542 Haiss A., Kümmerer K. (2006) Biodegradability of the X-ray contrast compound diatrizoic acid, identification
543 of aerobic degradation products and effects against sewage sludge micro-organisms Chemosphere 62:
544 294–302.
545 Hapeshi E., Lambrianides A., Koutsoftas P., Kastanos E.; Michael C., Fatta-Kassinos D. (2013) Investigating
546 the fate of iodinated X-ray contrast media iohexol and diatrizoate during microbial degradation in an MBBR
547 system treating urban wastewater; Environ. Sci. Pollut. Res. 20: 3592–3606
548 Howard P.H., Muir D.C.G. (2011) Identifying new persistent and bioaccumulative organics among chemicals
549 in commerce II: pharmaceuticals; Environ. Sci. Technol. 45: 6938–46
550 Kalsch W. (1999) Biodegradation of the iodinated X-ray contrast media diatrizoate and iopromide Sci. Total
551 Environ. 225: 143–153.
552 Kase R., Eggen R. I. L., Junghans M., Götz C., Hollender J. (2011) Assessment of Micropollutants from
553 Municipal Wastewater - Combination of Exposure and Ecotoxicological Effect Data for Switzerland, Waste
554 Water - Evaluation and Management Fernando Sebastian Garcia Einschlag (Ed.) InTech
555 Kormos J.L., Schulz M., Wagner M., Ternes T. A. (2009) Multistep Approach for the Structural Identification
556 of Biotransformation Products of Iodinated X-ray Contrast Media by Liquid Chromatography/Hybrid Triple

557 Quadrupole Linear Ion Trap Mass Spectrometry and 1H and 13C Nuclear Magnetic Resonance, Anal. Chem.,
558 81: 9216–9224
559 Kormos J.L., Schulz M., Kohler H.P.E., Ternes T.A. (2010) Biotransformation of selected iodinated x-ray
560 contrast media and characterization of microbial transformation pathways; Environ. Sci. Technol. 44: 4998-
561 5007
562 Kormos J.L., Schulz M., Kohler H.P.E., Ternes T.A. (2011) Occurrence of iodinated X-ray contrast media and
563 biotransformation products in the urban water cycle. Environ. Sci. Technol. 45: 8723-8732
564 Jeong J., Jung J., Cooper W. J., Song W. (2010) Degradation mechanisms and kinetic studies for the
565 treatment of X-ray contrast media compounds by advanced oxidation/reduction processes Water Res. 44:
566 4391-4398
567 Matsushita T., Kobayasgu N, Hashizuka M., Sakuma H., Kondo T., Matsui Y, Shirasaki N. (2015) Changes in
568 mutagenicity and acute toxicity of solutions of iodinated X-ray contrast media during chlorination.
569 Chemosphere 135: 101-107
570 Ning B., Graham N.J.D. (2008) Ozone Degradation of Iodinated Pharmaceutical Compounds. J. Environ. Eng.
571 134: 1-43
572 Ohmori T., Nakamura M., Tada S., Sugiyama T., Itoh, Y, Udagawa, Y, Hirano K. (2008) A highly sensitive
573 assay for ritodrine in human serum by hydrophilic interaction chromatography-tandem mass spectrometry.
574 J. Chromat. B: Analytical Technol. Biomed. Life Sci. , 861(1): 95-100
575 Parvez S., Venkataraman C., Mukherji S. (2006) A review on advantages of implementing luminescence
576 inhibition test (*Vibrio fischeri*) for acute toxicity prediction of chemicals; Environ. Int. 32: 265-268
577 Perez S., Eichhorn P., Celiz M.D., Aga D.S. (2006) Structural characterization of metabolites of the X-ray
578 contrast agent iopromide in activated sludge using ion trap mass spectrometry; Anal. Chem. 78 (6) 1866-
579 1874.
580 Pérez S., Eichhorn P., Ceballos V., Barceló, D., (2009) Elucidation of phototransformation reactions of the X-
581 ray contrast medium iopromide under simulated solar radiation using UPLC-ESI-QqTOF-MS. J. Mass.
582 Spectrom. 44: 1308–1317
583 Pitrè D., Felder E. (1980) Development, chemistry, and physical properties of iopamidol and its analogues.
584 Invest. Radiol. 15 (6): 301-9
585 Polo A.M.S., López-Peñalver J.J., Sánchez-Polo M., Rivera-Utrilla J., Velo-Gala I., Salazar-Rábago J.J. (2016)
586 Oxidation of diatrizoate in aqueous phase by advanced oxidation processes based on solar radiation. J.
587 Photochem. Photobiol. A: Chem. 319–32:0 87–95
588 Putschew A., Miehe U., Tellez A.S., Jekel M. (2007) Ozonation and reductive deiodination of iopromide to
589 reduce the environmental burden of iodinated X-ray contrast media. Water Science & Technology 56 (11):
590 159–165

591 Rastogi T., Leder C., Kümmerer K. (2014) Qualitative environmental risk assessment of photolytic
592 transformation products of iodinated X-ray contrast agent diatrizoic acid Sci. Total Environ. 482–483: 378–
593 388
594 Redeker M., Wick A., Meermann B., Ternes,T. A. (2014) Removal of the Iodinated X‑ray Contrast Medium
595 Diatrizoate by Anaerobic Transformation; Environ. Sci. Technol. 48: 10145−10154
596 Santos L.H.M.L. M., Gros M., Rodriguez-Mozaz S., Delerue-Matos C., Pena A., Barceló D., Montenegro
597 M.C.B.S.M. (2013) Contribution of hospital effluents to the load of pharmaceuticals in urban wastewaters:
598 Identification of ecologically relevant pharmaceuticals; Sci. Total Environ. 461−462: 302−316
599 Schulz M., Loeffler D., Wagner M., Ternes T.A. (2008) Transformation of the X-ray contrast medium
600 iopromide in soil and biological wastewater treatment; Environ. Sci. Technol. 42 (19): 7207-7217
601 Schymanski EL., Jeon J, Gulde R., Fenner K., Ruff M., Singer H.P., Hollender J. (2014) Identifying small
602 molecules via high resolution mass spectrometry: communicating confidence. Environ. Sci. Technol., 48 (4),
603 2097-2098
604 Seitz W., Jiang J.Q., Schulz W., Weber W.H., Maier D., Maier M. (2008) Formation of oxidation by-products
605 of the iodinated X-ray contrast medium iomeprol during ozonation; Chemosphere 70 (7): 1238-1246.
606 Seitz W., Weber W.H., Jiang J.-Q., Lloyd B.J., Maier M., Maier D., Schulz W. (2006) Monitoring of iodinated
607 X-ray contrast media in surface water. Chemosphere 64: 1318-1324
608 Sichel C., Garcia C., Andre K. (2011) Feasibility studies: UV/chlorine advanced oxidation treatment for the
609 removal of emerging contaminants. Water Res. 45 (19): 6371-6380
610 Simazaki D., Kubota R., Suzuki T., Akiba M., Nishimura T., Kunikane S. (2015) Occurrence of selected
611 pharmaceuticals at drinking water purification plants in Japan and implications for human health. Water
612 Res. 76:187-200
613 Singh R.R., Lester Y., Linden K.G., Love N.G., Ekin Atilla-Gokcumen G., Aga D.S. (2015) Application of
614 Metabolite Profiling Tools and Time-of-Flight Mass Spectrometry in the Identification of Transformation
615 Products of Iopromide and Iopamidol during Advanced Oxidation, Environ. Sci. Technol. 49: 2983−2990
616 Stuart M., Lapworth D., Crane E., Hart A.(2102) Review of risk from potential emerging contaminants in UK
617 groundwater; Sci. Total Environ. 416: 1–21
618 Sugihara M.N., Moeller D., Paul T., Strathmann T.J. (2013) TiO_2-photocatalyzed transformation of the
619 recalcitrant X-ray contrast agent diatrizoate; Appl. Catal. B: Environ. 129: 114– 122
620 Ternes T.A., Hirsch R. (2000) Occurrence and Behavior of X-ray Contrast Media in Sewage Facilities and the
621 Aquatic Environment; Environ. Sci. Technol., 34: 2741-2748
622 Ternes T.A., Stüber J., Herrmann N., Mcdowell D., Ried A., Kampmann M., Teiser B. (2003) Ozonation: a tool
623 for removal of pharmaceuticals, contrast media and musk fragrances from wasterwater? Water Res.
624 37:1976-1982.

625 Ternes T.A., Bonerz M., Hermann n., Teiser B, Andersen H.R. (2007) Irrigation of treated wastewater in
626 Braunschweig, Germany: an option to remove pharmaceuticals and musk fragrances. Chemosphere 66:
627 894-904
628 Tian F., Xu B., Lin Y., Hu C., Zhang T., Gao N. (2014) Photodegradation kinetics of iopamidol by UV
629 irradiation and enhanced formation of iodinated disinfection by-products in sequential oxidation processes.
630 Water Res. 58: 198-208
631 Węgrzyn A., Żabczyński S. (2014) Monitoring of bacterial biodiversity in anaerobic membrane bioreactors
632 (mbrs) dealing with wastewater containing x-ray contrast media compounds. Environ. Protect. Engineer. 40
633 (1): 151-164
634 Wendel F.M., Eversloh C.L., Machek E.J., Duirk S. E, Plewa M.J., Richardson S.D., Ternes T.A. (2014)
635 Transformation of Iopamidol during Chlorination.. Environ. Sci. Technol. 48: 12689-1269
636 Wendel F.M., Ternes T.A. Richardson S.D., Duirk S. E, Wagner E.D.., Plewa M.J., (2016) Comparative Toxicity
637 of High-Molecular Weight Iopamidol Disinfection Byproducts, Environ. Sci. Technol. Lett. 3: 81−84
638 www.vah.com/assets/1/public_works/Understanding_Your_Sewer.pdf, accessed June 27, 2016.
639 Zhao C., Arroyo-Mora L.E., DeCaprio, A.P., Sharma, V.K., Dionysiou, D.D., O'Shea K. E. (2014) Reductive and
640 oxidative degradation of iopamidol, iodinated X-ray contrast media, by Fe(III)-oxalate under UV and visible
641 light treatment. Water Res. 67: 144-153
642 Zonja B., Delgado A., Pérez S., Barceló D. (2015) LC-HRMS Suspect Screening for Detection-Based
643 Prioritization of Iodinated Contrast Media Photodegradates in Surface Waters, Environ. Sci. Technol. 49:
644 3464−3472
645

646 # Tables

Sampling Site	Date Sampled
Bertau (Chicago River)	April 21 2015
Kirie WWTP	April 23 2015
Stickney WWTP	May 7 2015
Weed Street (Chicago River)	May 12 2015
Kirie WWTP	May 14 2015

647 **Table 1:** Sites and Dates for Water Samples used in this Study.

648

[M+H$^+$]	Empirical formula	Name	Δmmu	t_R (min.)
777.8688	$C_{17}H_{23}O_8N_3I_3$	IO	7.430	4.7
1406.6453	$C_{28}H_{33}O_{12}N_6I_6$	IO-1407	3.355	27.9
793.8632	$C_{17}H_{23}O_9N_3I_3$	IO-794	-2.525	5.5
778.8619	$C_{17}H_{22}O_9N_2I_3$	IO-779	16.554	4.5
775.8430	$C_{17}H_{21}O_8N_3I_3$	IO-776	-2.760	4.2
735.8124	$C_{14}H_{17}O_8N_3I_3$	IO-736	-2.040	10.6
705.8377	$C_{14}H_{19}O_6N_3I_3$	IO-706	-2.531	6.0
704.8061	$C_{14}H_{16}O_7N_2I_3$	IO-705	-2.516	4.8
661.7763	$C_{11}H_{11}O_6N_3I_3$	IO-662	-1.331	11.8
651.9627	$C_{17}H_{24}O_8N_3I_2$	IO-652	-2.027	4.6
649.9467	$C_{17}H_{22}O_8N_3I_2$	IO-650	-2.357	4.2
635.9096	$C_{16}H_{20}O_8N_3I_2$	IO-636	20.252	6.0
631.8011	$C_{11}H_{13}O_4N_3I_3$	IO-632	-2.371	6.0
614.7746	$C_{11}H_{10}O_4N_2I_3$	IO-615	-2.312	6.3
579.9407	$C_{14}H_{20}O_6N_3I_2$	IO-580	-2.868	5.9
576.8940	$C_{14}H_{15}O_7N_2I_2$	IO-577	-2.333	4.7
544.8678	$C_{13}H_{11}O_6N_2I_2$	IO-545	-2.239	6.0
540.7379	$C_9H_4O_3I_3$	IO-541	-2.343	6.6
504.8735	$C_{11}H_{11}O_5N_2I_2$	IO-505	-1.684	4.7
486.8646	$C_{11}H_9O_4N_2I_2$	IO-487	-2.529	4.8
384.9656	$C_{13}H_{10}O_4N_2I$	IO-385	-2.426	4.4
366.9567	$C_{13}H_8O_3N_2I$	IO-367	-1.290	9.8
331.9601	$C_{10}H_7O_4NI$	IO-332	18.683	4.8
330.9549	$C_{10}H_8O_3N_2I$	IO-331	-2.362	4.7

Table 2. Transformation products formed from iopamidol (IO) with TiO_2 P25 200 mg/l.

[M+H$^+$]	Empirical formula	Name	Δmmu	t_R (min)
791.8777	$C_{18}H_{25}O_8N_3I_3$	IP	0.670	4.7
759.8520	$C_{17}H_{21}O_7N_3I_3$	IP-760	1.185	3.7
727.8254	$C_{16}H_{17}O_6N_3I_3$	IP-728	-0.071	3.8
681.9783	$C_{18}H_{26}O_9N_3I_2$	IP-682	2.978	2.8
665.9812	$C_{18}H_{26}O_8N_3I_2$	IP-666	0.823	3.6
651.9652	$C_{17}H_{24}O_8N_3I_2$	IP-652	0.423	3.2
554.0627	$C_{18}H_{25}O_9N_3I$	IP-554	-0.259	3.6
531.8993	$C_{10}H_{16}O_8NI_2$	IP-532	5.774	3.7
526.0678	$C_{17}H_{25}O_8N_3I$	IP-526	-0.274	2.8
466.0476	$C_{15}H_{21}O_6N_3I$	IP-466	0.685	4.7
452.0313	$C_{14}H_{19}O_6N_3I$	IP-452	0.005	3.5

655 **Table 3**. Transformation products formed from iopromide (IP) with TiO_2 P25 200 mg/l.

[M+H$^+$]	Empirical formula	Name	Δmmu	t_R (min.)
614.7748	$C_{11}H_{10}O_4N_2I_3$	DTZ	-0.027	18.3
630.7718	$C_{11}H_{10}O_5N_2I_3$	DTZ-631	-0.027	16.0
586.7796	$C_{10}H_{10}O_3N_2I_3$	DTZ-587	-2.98	14.7
573.7480	$C_9H_7O_4NI_3$	DTZ-574	-2.373	8.2
488.8804	$C_{11}H_{11}O_4N_2I_2$	DTZ-489	-0.101	7.7
486.8624	$C_{11}H_9O_4N_2I_2$	DTZ-487	-2.235	7.3
470.8690	$C_{11}H_9O_3N_2I_2$	DTZ-471	-0.705	7.2
403.8489	$C_8H_8O_2NI_2$	DTZ-404	-2.405	9.5
362.9722	$C_{11}H_{12}O_4N_2I$	DTZ-363	-11.456	7.9
332.9705	$C_{10}H_{10}O_3N_2I$	DTZ-333	-2.542	9.6
318.9550	$C_9H_8O_3N_2I$	DTZ-319	-2.422	9.1

656 **Table 4**. Transformation products of diatrizoate (DTZ) with TiO_2 P25 200 mg/l.

657

	DTZ (µg/l)	IO (µg/l)	IP (µg/l)
BERTEAU	n.d.	0.56±0.05	0.16±0.02
KIRIE BEFORE	0.28±0.03	0.98±0.08	0.23±0.02
KIRIE AFTER	n.d.	0.091+0.010	n.d.
WEED STREET	n.d.	0.07±0.01	0.020±0.003
STICKNEY	0.055±0.005	0.63±0.02	n.d.

Table 5. ICMs concentration in wastewater and river water.